AN UNSTRUCTURED FINITE VOLUME SOLVER FOR TWO PHASE WATER/VAPOUR FLOWS BASED ON AN ELLIPTIC ORIENTED FRACTIONAL STEP METHOD

N. Méchitoua*, M. Boucker, J. Lavièville
EDF R&D
Département Mécanique des Fluides et Transferts Thermiques
6, Quai Watier - 78400 Chatou Cedex France

S. Pigny, G. Serre
CEA DEN DTP
Service d'études et de Modélisation en THermohydraulique
17, rue des Martyrs - 38054 Grenoble Cedex 9, France

Abstract

Based on experience gained at EDF and CEA, a more general and robust 3D multiphase flow solver is being currently developped for over three years. This solver, based on an elliptic oriented fractional step approach, is able to simulate multicomponent/multiphase flows.

Discretization follows a 3D full unstructured finite volume approach, with a collocated arrangement of all variables. The non linear behaviour between pressure and volume fractions and a symmetric treatment of all fields are taken into account in the iterative procedure, within the time step. It greatly enforces the realizability of volume fractions (i.e $0<\alpha<1$), without artificial numerical needs.

Applications to widespread test cases are shown to assess the accuracy and the robustness of the flow solver in different flow conditions, encountered in nuclear reactors pipes.

Corresponding author
E-mail : namane.mechitoua@edf.fr
Phone : 01.30.87.80.27
Fax : 01.30.87.72.53

Introduction

Multiphase flows can be encountered in many industrial devices. Understanding the thermalhydraulics behavior of such devices is important, in order to predict the effects of the modifications of components on the general efficiency and the safety of the installations. Numerical modelling can be a suitable tool for understanding and predict such complex physical phenomena.

Numerical simulation combined with physical modelling is essential in nuclear engineering. Indeed, it does not exist simplified and predictive scaling laws for the main processes which would allow a direct transfer of results from small scale test facilities to the full size device.

The increase in performance of computer hardware makes possible the 3D simulation of multiphase flows, with energy and mass transfers, as liquid water/ vapour water flows for instance. Of course, direct simulation of the instantaneous multiphase flow fields is not yet practical for engineering studies. It is often necessary to filter the small characteristics lengths, in a physical or numerical way. From a physical point of view, averaged governing equations lead to a new system. Closure laws must be provided by physicists for new expressions of fluctuating quantities that appear in the averaged equations. From a numerical point of view, instantaneous equations can be solved for characteristics lengths greater than the mesh size.

This paper deals with a 3D multiphase flow solver developped in the EDF/CEA NEPTUNE software /ref. 1/. The paper is organised in the following manner. Firstly, governing equations are presented, in an averaged form, with the main physical modelling currently used for benchmarking and studies. Secondly, the mass/ momentum /energy coupling algorithm is explained. Presentation is then focused on Poisson equation on Pressure variable, which “gathers” all the couplings between all variables. Thirdly, numerical schemes used for space discretisation based on a finite volume approach and data structure are presented. Endly, widespread testcases concerning water/vapour flows with energy and mass transfers are shown to assess the robustness of the solver in different flow conditions. In conclusion, some directions of improvement are listed.

Governing Equations

Based on experience gained at EDF and CEA, a more general and robust multiphase flow solver is being currently developped for over three years /ref. 2/. This new solver, based on an elliptic approach, is able to simulate multicomponent multiphase flows. The multi-fluid set of equations is an extension of the “two fluid – one pressure” model to the case of m phases. Each field (fluid component and/or phase) is modelled through at least 3 conservation equations representing mass, momentum and total enthalpy.

$$\frac{\partial \alpha_k \rho_k}{\partial t} + \mathrm{div}(\alpha_k \rho_k \vec{U}_k) = \Gamma_k \tag{1}$$

$$\frac{\partial \alpha_k \rho_k \vec{U}_k}{\partial t} + \mathrm{div}\vec{}(\vec{U}_k \otimes \alpha_k \rho_k \vec{U}_k) = \mathrm{div}\vec{}(\alpha_k \bar{\bar{\tau}}_k + \bar{\bar{\Sigma}}_k) - \alpha_k \vec{\nabla} P + \vec{I}_k' + \Gamma_k \vec{U}_k + \alpha_k \rho_k \vec{g} + \alpha_k \vec{S}_k \tag{2}$$

$$\frac{\partial \alpha_k \rho_k H_k}{\partial t} + \mathrm{div}(\alpha_k \rho_k \vec{U}_k H_k) = \mathrm{div}(\alpha_k \lambda_k \vec{\nabla} T_k) + \mathrm{div}((\alpha_k \bar{\bar{\tau}}_k + \Sigma_k)\vec{U}_k) + \alpha_k \frac{\partial P}{\partial t} + \vec{U}_k . \vec{I}_k' + \alpha_k \rho_k \vec{g} . \vec{U}_k + \Gamma_k H_k + \Pi_k' \tag{3}$$

The volume fractions relation ($\sum \alpha_k = 1$) and the jump conditions on mass($\sum \Gamma_k = 0$), momentum ($\vec{I}'_k$) and energy (Π'_k) are added to this set of equations. Note that the energy variable is in fact the total enthalpy ($H_k = e_k + 0.5\vec{U}_k^2 + P/\rho_k$). Hence, we solve (5m +1) following physical variables (α_k, U_k, H_k, P), which is workable by considering the above mentioned system of (5m +1) equations (5m balance equations and the constraint on volume conservation).

In the above equations, interface velocity between phases are supposed to be close to the velocity of the *m* present phases. This hypothesis is suitable for droplets or heavy particle, but it is questionable for bubbles. I'_k represent the momentum interfacial transfer between all phases p different from k and the considered phase k. In general, works of buyoancy and viscosity forces in the total enthapy equation (3) are negligible and are not taken into account in the computations.

Notice that :

$\bar{\bar{\tau}}_k = \mu_k (\bar{\bar{\nabla}}\vec{U} + {}^t\bar{\bar{\nabla}}U)$ is the laminar viscous constraint tensor,

$\bar{\bar{\Sigma}}_k = -\left\langle \alpha_k \rho_k \vec{U}''_k \otimes \vec{U}''_k \right\rangle$ is the turbulent constraint tensor.

$\vec{I}'_k$ represents the momentum interfacial transfer of all phases p to the phase k (drag, added mass, turbulent contributions to drag and adde mass, …) : $\vec{I}'_k = \sum_{p \neq k} \vec{I}'_{p \to k}$.

Π'_k represents the heat transfer between phases. In the important particular case of liquid water/vapour water flows with mass transfer due to heat transfer, these terms are written in the following form :

$$\Pi'_k = \Pi_k - \Gamma_k H_k \ , \ \sum_k \Pi_k = 0 \ , \ \Pi'_k = -\xi_k (T_k - T_{sat}) \qquad (4)$$

Heat transfer coefficients ξ_k depend on the models of nucleate boiling, condensation and evaporation. These coefficients are nils if there is no heat transfer.

Additive equations for each field can be used in order to model physics, such as turbulence, phase separation, inclusions diameters, nucleate boiling near walls and radiation heat transfer.

The modified k-epsilon model for continuous phases and the local equilibrium model of Tchen are the most used turbulence models for taking into account turbulent dispersion /ref. 3/. These models are written in the following form :

$$\frac{\partial \alpha_k \rho_k q_k^2}{\partial t} + \mathrm{div}(\alpha_k \rho_k \vec{U}_k q_k^2) = \mathrm{div}(\alpha_k \frac{\mu_k^t}{\sigma_k} \vec{\nabla} q_k^2) + P_k - \alpha_k \rho_k \varepsilon_k$$

$$\frac{\partial \alpha_k \rho_k \varepsilon_k}{\partial t} + \mathrm{div}(\alpha_k \rho_k \vec{U}_k \varepsilon_k) = \mathrm{div}(\alpha_k \frac{\mu_k^t}{\sigma_\varepsilon} \vec{\nabla} \varepsilon_k) + C_{\varepsilon 1} \frac{\varepsilon_k}{q_k^2} P_k - C_{\varepsilon 2} \alpha_k \rho_k \varepsilon_k \qquad (5)$$

P_k is the turbulent production term, written as : $P_k = -\left\langle \alpha_k \rho_k U''_{k,i} U''_{k,j} \right\rangle (\partial U_{k,i} / \partial x_j)$

The influence of turbulence between phases is taken into account through correlations which modify the turbulent viscosity. The correlations depend on turbulence quantities of each phase, such

as turbulent kinetic energy and turbulent dissipation, the covariance of the fluctuating velocities and the turbulent characteristic time scale of the droplet and bubbles.

Mass/momentum/energy coupling

The mass /momentum /energy coupling can be seen as an extension of the well known pressure-based method used in one phase flow solver. In our approach, mass, momentum and energy are coupled by an iterative procedure within the time step. The second group of variables, coming from physical modelling of primitive equations of mass, momentum and energy, are weakly coupled with the pressure, velocity components and volume fractions. Examples of such variables are turbulence quantities (such as turbulent kinetic energy and turbulent dissipation energy) and interfacial areas.

The complete system defined in the previous section is solved in three major fractional steps, within the time step :

- the first one concerns a prediction of velocities through the momentum equations;
- the second one concerns the coupling between volume fractions, pressure and energy through mass energy equations and a simplified form of momentum equations;
- the third one concerns the computations of "secondary" variables, such as turbulence quantities and interfacial areas. This step depends from the two first steps.

The two first steps are detailed above.

Velocities prediction step.

During that step, 3m convection/diffusion equations with source terms are solved, one for each velocity component of each phase. All others variables as pressure, volume fractions, turbulence characteristics are "frozen" to the values of the previous time step. These equations derived from partially linearised momentum equations, written for each increment $\delta U_k^* = U_k^* - U_k^n$, in the following form :

$$\begin{aligned}&\rho_k^n \frac{\delta\vec{U}_k^*}{\Delta t} - \delta\vec{U}_k^* \,\mathrm{div}(\alpha_k^n \rho_k^n \vec{U}_k^n)/\alpha_k^n + \mathrm{div}(\delta\vec{U}_k^* \otimes \alpha_k^n \rho_k^n \vec{U}_k^n)/\alpha_k^n \\ &+ \mathrm{div}(-\alpha_k^n \mu_{k,e}^n \nabla\delta\vec{U}_k^*)/\alpha_k^n - \sum_{l=l}^{m} \frac{\bar{\bar{\partial}}(\vec{I}'_k/\alpha_k + \vec{S}_k)^n}{\partial\vec{U}_l}\delta\vec{U}_l^* = \vec{B}_k^{exp}\end{aligned} \tag{6}$$

$$\begin{aligned}\vec{B}_k^{exp} &= \vec{U}_k^n \mathrm{div}(\alpha_k^n \rho_k^n \vec{U}_k^n)/\alpha_k^n - \mathrm{div}(\vec{U}_k^n \otimes \alpha_k^n \rho_k^n \vec{U}_k^n)/\alpha_k^n \\ &- \mathrm{div}(-\alpha_k^n \mu_{k,e}^n (\nabla\vec{U}_k^n + {}^T\nabla\vec{U}_k^n))/\alpha_k^n - \vec{\nabla}P^n + \rho_k^n\vec{g} + \vec{I}'^n_k/\alpha_k^n + \vec{S}_k^n\end{aligned} \tag{7}$$

In that system, the jacobian matrices $\bar{\bar{\partial}}(\vec{I}'_k/\alpha_k + \vec{S}_k)/\partial\vec{U}_l$ represent the implicit part of the interfacial transfer terms and source terms, which are taken into account only if they act as return-to-equilibrium terms and are easy to derive.

These equations are then discretised on a finite number of cells. Differential terms are integrated, following the Green-Ostrogradski formula, which leads to surface integrals. Note that the equations are previously divided by volume fractions, defined in the cells. Convective and diffusive fluxes are modified in order to avoid "infinite" values, when volume fractions tend towards zero.

Mass-momentum-energy coupling

During this step, the advective and diffusive parts of the momentum equations are "frozen" through the predicted velocities $\vec{U}_k^*$, while the local and first order differential terms, depending of pressure and volume fractions, "frozen" during the velocities prediction step, are taken into account, in an implicit way. Once obtains a reduced form of momentum equation, written in the following manner :

$$\alpha_k^{n+1}\rho_k^n\frac{\vec{U}_k^{n+1}-\vec{U}_k^*}{\Delta t}-\sum_{l=1}^{m}\left(\frac{\bar{\bar{\partial}}\vec{TS}_k}{\partial\vec{U}_l}\right)^n(\vec{U}_k^{n+1}-\vec{U}_k^*)-\sum_{l=1}^{m}\left(\frac{\partial\vec{TS}_k}{\partial\alpha_l}\right)^n\delta\alpha_l^{n+1}$$
$$+\sum_{l=1}^{m}\left(\frac{\bar{\bar{\partial}}\vec{TS}_k}{\partial(\nabla\alpha_l)}\right)^n\nabla\delta\alpha_l^{n+1}+\alpha_k^{n+1}\nabla\delta P^{n+1}=0,\quad\text{with }\delta\alpha_l^{n+1}=\alpha_l^{n+1}-\alpha_l^n \tag{8}$$

where $\bar{\bar{TS}}_k^*$ gathers the interfacial momentum transfer and other source terms.

In this steps, equations (8) are coupled with the mass and energies equations, whose time discretisations have the following form :

$$\frac{\alpha_k^{n+1}\rho_k^{n+1}-\alpha_k^n\rho_k^n}{\Delta t}+\mathrm{div}(\alpha_k^{n+1}\rho_k^n\vec{U}_k^{n+1})=\Gamma_k^{n+1} \tag{9}$$

$$\frac{\alpha_k^{n+1}\rho_k^{n+1}H_k^{n+1}-\alpha_k^n\rho_k^nH_k^n}{\Delta t}+\mathrm{div}(\alpha_k^{n+1}\rho_k^n\vec{U}_k^{n+1}H_k^{n+1/2}-\alpha_k^n\lambda_k^n\vec{\nabla}T_k^{n+1})=$$
$$\Gamma_k^{n+1/2}H_k^{n+1/2}+\Pi_k'^{n+1/2}+\alpha_k^{n+1/2}\frac{P^{n+1}-P^n}{\Delta t} \tag{10}$$

Thermodynamic and thermochemistry tables give the bijective relation between the temperatures T_k and thermal enthalpies $h_k = H_k - 1/2\ \rho\ U^2$.

There are several possibilities, concerning the degree of coupling of equations (8), (9) and (10), via the implicitation of different terms. Our main applications concern incompressible or low Mach number two phase flows, with possibility of high heat and mass transfer between the two phases. From this point of view, it is necessary, at least :

- to implicit velocities in the mass equations and pressure in the momentum equations, in order to fit the Courant number to material velocity rather than to the acoustic speed,
- to predict at best, "residual" or lightest phases as vapour or air,
- to implicit at best, the coupling due to heat and mass transfers, which depends, in a strong non linear manner, on pressure, energies and volume fractions.

Velocities variables are eliminated, by introducing the reduced momentum equations in the mass equations. Additional simplifications are necessary for obtaining tractable coupled equations between pressure and volume fractions. To this end, implicit coupling between void fractions inside the space divergence are not taken into account in equations (8). This leads to a m equations non linear system for pressure P^{n+1} and volume fractions α_k^{n+1} :

$$\frac{\alpha_k^{n+1}\rho_k^{n+1}-\alpha_k^n\rho_k^n}{\Delta t}+\mathrm{div}\left\{\alpha_k^{n+1}\rho_k^n\left(\vec{w}_k-\overline{\overline{K}}_k\vec{\nabla}\alpha_k^{n+1}-\overline{\overline{D}}_k\vec{\nabla}P^{n+1}\right)\right\}=\Gamma_k^{n+1} \qquad (11)$$

with :

$$\alpha_k^{n+1}\rho_k^n\vec{U}_k^{n+1}=\alpha_k^{n+1}\rho_k^n\left(\vec{w}_k-\overline{\overline{K}}_k\vec{\nabla}\alpha_k^{n+1}-\overline{\overline{D}}_k\vec{\nabla}P^{n+1}\right) \qquad (11)\text{ bis}$$

System (11) is closed by the volume conservation constraint : $\sum_{k=1}^{m}\alpha_k^{n+1}=1$ (11) ter

Of course, the volume conservation constraint of the previous time step is already respected.

The above (10) and (11) equations are solved, thanks to an iterative and fractional step procedure which is summarized below :

Initialisation :

$$i=0,\ P^{(i)}=P^n,\ \alpha_k^{(i)}=\alpha_k^n,\ H_k^{(i)}=H_k^n,\ \vec{U}_k^{(i)}=\vec{U}_k^*,\ \rho_k^{(i)}=\rho_k\left(P^{(i)},h_k^{(i)},....\right) \qquad (12)$$

Iterations :

(0) – indice increment

$i = i + 1$

(1) – Enthalpies prediction for all phases – Thermodynamics properties updating.

Equations (10) are solved for the unknown $H_k^{(i)}$. All others terms are "frozen" and correspond to the previous iteration (i-1). Heat transfers source terms are implicited according to the unknown enthalpies, if they act as return to equilibrium terms. An additional substep can be necessary, in order to simply couple the enthalpies, due to the implicit linearisation of the source terms.

Then, thermodynamics properties (densities, molecular viscosities and diffusivities, specific heat, …) are updated in the following form : $\rho_k^{(i)}=\rho_k\left(P^{(i)},h_k^{(i)},....\right)$, $\lambda_k^{(i)}=\lambda_k\left(P^{(i)},h_k^{(i)},....\right)$, ...

(2) – Volume fractions predictions

Equations are solved for the unknowns $\alpha_k^{(i)}$. An additional substep can be necessary, in order to locally couple the volume fractions between themselves, due to the implicit coupling of the source terms.

$$\frac{\alpha_k^{(i)}\rho_k^{(i)}-\alpha_k^n\rho_k^n}{\Delta t}+\mathrm{div}\left\{\alpha_k^{(i)}\rho_k^n\left(\vec{w}_k-\overline{\overline{D}}_k\vec{\nabla}P^{(i)}\right)-\alpha_k^{(i-1)}\rho_k^n\overline{\overline{K}}_k\vec{\nabla}\alpha_k^{n+1}\right\}=\Gamma_k^{(i)} \qquad (13)$$

A special care has to be taken when discretising the source terms, in order to avoid negative values of volume fractions. The convective and diffusive parts of the above equations, respectively discretised with suitable upwinding and diffusive schemes, preserve the positivity of the unknown $\alpha_k^{(i)}$.

(3) – Correction step with a pressure equation. Velocities updating.

If the predicted volume fractions, which are all positives, do not respect the volume conservation constraint (11) ter, a correction step is needed for adjusting velocities through the gradient of the pressure increment $-\overline{\overline{D}}_k\vec{\nabla}\delta P^{(i)}$.

$$\frac{\alpha_k^{(i+1/2)}\rho_k^{(i+1/2)} - \alpha_k^{(i)}\rho_k^{(i)}}{\Delta t} + \mathrm{div}\left\{-\alpha_k^{(i)}\rho_k^{n}\overline{\overline{D}}_k\vec{\nabla}\delta P^{(i)}\right\} = \Gamma_k^{(i+1/2)} - \Gamma_k^{(i)} \qquad (14)$$

All unknowns $\alpha_k^{(i+1/2)}, \rho_k^{(i+1/2)}, \Gamma_k^{(i+1/2)}$ are expressed in function of pressure increment $\delta P^{(i)}$, using, in a simplified manner, the above equations, the equations of energies and the equations of state. Then, by prescribing $\sum_k \alpha_k^{i+1/2} = 1$, we obtain an elliptic pressure equation on pressure increment, whose right hand side is proportional to default or excess predicted volume $\left(-1 + \sum_k \alpha_k^{i+1/2}\right)$.

Pressure and velocities (either on cell and face location) are updated through :

$$\begin{aligned} P^{(i)} &= P^{(i)} + \delta P^{(i)} \\ \vec{U}_k^{(i)} &= \vec{w}_k - \overline{\overline{K}}_k\vec{\nabla}\alpha_k^{(i)} - \overline{\overline{D}}_k\vec{\nabla}P^{(i)} \end{aligned} \qquad (15)$$

It can be noticed that volume fractions and thermodynamic properties are not systematically updated in this step, because this updating can violate the minimum principle for volume fractions, which is respected in the prediction step (2).

(4) – convergence test

The overall convergence of the procedure is controlled by a test on the predicted volume constraint.

If Max $\left|1 - \sum_{k=1}^{m}\alpha_k^{(i)}\right| \le \varepsilon$, then the iterative procedure stops and :

$$P^{n+1} = P^{(i)},\ \alpha_k^{n+1} = \alpha_k^{(i)},\ H_k^{n+1} = H_k^{(i)},\ \vec{U}_k^{n+1} = \vec{U}_{k,}^{(i)}\ \rho_k^{n+1} = \rho_k^{(i)} \qquad (16)$$

else, go back to step (0).

When the procedure converges, all increment should tend towards zero and the volume constraint is satisfied. If the procedure does not converge for a given number of cycles (~10) and a given precision on volume conservation constraint (~10^{-8}), the time step is reduced and the procedure is restarted.

It exists several ways to couple equations (10) and (11), see /ref. 4/. The presented approach, based on a global phasic continuity, is suitable for obtaining a very good balance for each mass conservation equation, with or without mass transfer term. But when strong coupling is lacking, the lighter fluid will change disproportionately and both volume fractions will change in the same direction, in response to the same pressure gradient adjustement. That's why, it is necessary to enforce the link between the momentum equations, before resolving mass equations. The local matrices $\overline{\overline{K}}_k, \overline{\overline{D}}_k$ per cell, may be non diagonal and non isotropic (matrices 3*3). They may contain the implicit coupling, due to inertia forces, interfacial momentum transfers and other source terms, in a simplified form. This permits to overcome some defaults of the method and to insure a rather good rate of convergence.

Data structure, space discretisation, linear system resolution.

Spatial discretisation is based upon a three dimensional full unstructured finite volume approach. A face based data structure allows the use of arbitrary shaped cells as tetrahedron, hexahedron, prism

and pyramids, including non matching cells. The discrete face separates two cells, as it is illustrated in figure 1. The face to cell connectivity is, for example, considering that surfaces are outing from cell I to the neighbours cells J1, J2 and J3 :

$$\begin{aligned} &J1 = IFACEL(1, N1);\ J2 = IFACEL(1,N2)\ ;\ J3 = IFACEL(1, N3) \\ &I\ = IFACEL(2,N1) = IFACEL(2,N2) = IFACEL(2,N3) \end{aligned} \qquad (17)$$

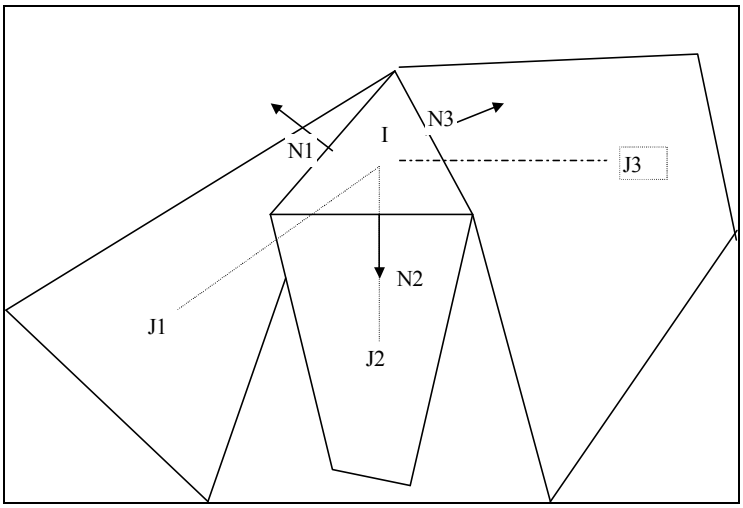

Figure 1 : view of cell's shape, and data structure

The data structure, used for CFD computations, contains, at least, the face to cell connectivity, the vectorial surfaces, the coordinates of points "associated" to cells and coordinates of gravity centers of faces, the attributes of the boundary faces. Non plane surfaces are shared in plane surface in order to have a finite volume scheme, at least, at first order in space.

All variables are collocated at the cell "centers". The cells can be built, from the primitive mesh or around the vertices of the primitive mesh. The main advantage of the primitive mesh is that it authorizes in a simpler manner, non matching mesh, with hanging nodes. The main advantage of the mesh built around the cell vertices is its superior "numerical" quality, if the primitive mesh is highly irregular and non orthogonal. The optimal location of the cell "center", from a numerical point of view, is not necessary at the geometric gravity center of the cell. It depends on the numerical scheme and the physical phenomena. The orthocenter is preferred to geometric gravity center, if it is located inside the cell.

Numerical consistency and precision for diffusive and advective fluxes for non orthogonal and irregular cells are taken into account through a gradient reconstruction technique. For example, we show below the numerical sketch of the diffusive flux built at first order, for smooth solutions /ref. 5/.

$$-(K\vec{\nabla}C)^{f}_{IJ}.\vec{N}_{IJ} = \frac{K_{IJ}(C_I - C_J) + (\overrightarrow{II'} - \overrightarrow{JJ'}).(K\vec{\nabla}C)^{c}_{IJ}}{I'J'}\left|\vec{N}_{IJ}\right| \qquad (18)$$

with $$(K\vec{\nabla}C)^{c}_{IJ} = \frac{1}{2}(K_I\vec{\nabla}C_I + K_J\vec{\nabla}C_J)\ ,\ K_{IJ} = \frac{2K_I K_J}{K_I + K_J}\ ,$$

and $\vec{N}_{IJ}$: vectorial surface separating cell I and cell J.

Note that for smooth solutions, an arithmetic interpolation of the diffusive coefficient, at the face center, is preferred to an harmonic interpolation.

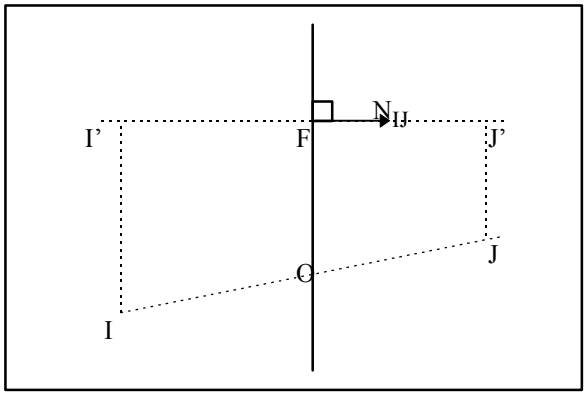

Figure 2
Diffusion scheme reconstructed at first order at face center F

Convective schemes for all variables, except pressure, are centered/upwind scheme. The switch between upwinded and centered interpolation is controlled by a slope test which detects the non monotony of the variable in the vicinity of the interpolation location. This switch acts as a flux limiter. Velocities components can be computed with a full centered scheme, because they are not subject to maximum and minimum principles.

Gradients are calculated at second order for regular cells and, at least, at first order for highly irregular cells /ref. 6/. An iterative finite volume procedure is preferred to the least square method because it produces smoother gradients on irregular cells.

A careful treatment of gradient terms of momentum equation is needed, in order to avoid spurious oscillations of pressure, velocity components and volume fractions, during the coupling of mass and momentum equations. This behaviour comes from the collocated arrangements of all variables for low speed flows and centered interpolations of variables at face centers. Variants of Rhie & Chow Interpolation /ref. 7/ are used for the gradient calculations, during the correction step presented at the previous section.

A special upwinded interpolation at face center for pressure gradient is needed, in order to take into account the stratified behaviour of the flow, due to buyoancy forces. The arithmetic coefficients of the face interpolation are weighted by the specific volume of the fluid.

$$\vec{\nabla} P_I \, \Omega_I = \sum_{J \in V_I} P_{IJ} \, \vec{N}_{IJ}, \quad P_{IJ} = \frac{A_{IJ} \, P_I / \rho_I + (1 - A_{IJ}) \, P_J / \rho_J}{A_{IJ} / \rho_I + (1 - A_{IJ}) / \rho_J}, \qquad (19)$$

$$\text{with } \rho = \sum_{k=1}^{\text{phase}} \alpha_k \rho_k \quad \text{and} \quad A_{IJ} = \text{geometric weight}$$

Phase residual management is a difficult task, from a numerical point of view. Perfect and elegant solutions do not exist at the moment. Our procedure consist to divide all conservative equations, except mass conservation equations, by volume fractions computed in the cells and to manage the behaviour of the face interpolated volume fractions in order to avoid “infinite” values. The upwind/ centered interpolation of volume fractions switches to an harmonic interpolation when

the volume fractions tend towards zero. The conservation of variables is not ruined, because there is no variable clipping. We proceed only to a modification of the fluxes, at the interfaces.

A large amount of linear systems have to be solved during the velocities prediction step and the mass/ momentum/ energy coupling. These systems, generally diagonal dominant, are solved by simple iterative methods :

- relaxation methods as Jacobi or Gauss Seidel for convective dominant systems,
- gradient methods as Preconditoned Conjugate Gradient, Stabilized Biconjugate Gradient and Conjugate Gardient Square for elliptic dominant systems.

Acceleration techniques, as Polynomial Preconditioners and algebraic multigrid solvers, are used.

Assessment of the numerical method.

Several widespread benchmark test cases, defined in /ref.8/, are performed in order to assess the accuracy and the robustness of the numerical method. We show below three examples of test cases performed by the solver.

The 1D static sedimentation test case /ref.9/:

The sedimentation of a mixture of water and air in a vertical tube is considered. Initially, void fraction is set to 0.5. Due to gravity, two volume fractions front propagates, one from the bottom going upwards, one from the top going downwards. Symmetrical momentum transfer is taken into account (drag and added mass). Figure 3 shows the gas volume fraction evolution with time. Realizability conditions on the volume fractions are satisfied with any artificial numerical needs and, once the steady state is reached, the solution remains stable. The steady pressure profile is in very good agreement with the analytical solution. The computation has been performed with two meshes of 74 and 149 cells.

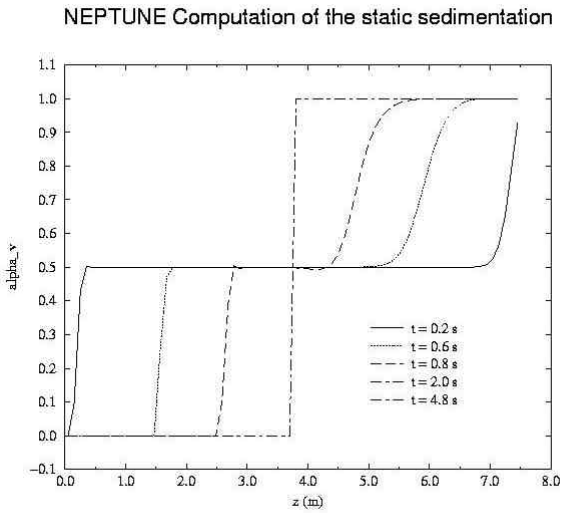

Figure 3 : Static sedimentation computation

Water Hammer Test Case /ref.10/ :

The Water Hammer experiment consists of a vertical tank of large dimensions connected via the bottom to a slightly sloping pipeline 36 m long with 19.05 mm diameter equipped with a valve at its downstream end, in the opposite direction from the tank. The experimental initial conditions are the followings :

- Pressure in the pipeline and the tank = 10 bars,
- Horizontal velocity in the pipeline = 0.401 m/s,
- Temperature = 163 ° Celsius.

A transient flow is initialised by fast closure of the valve. The phenomena observing during the transient are propagation of pressure waves, flashing and condensation due to the pressure variation on each side of saturation. Figure 4 shows the unsteady behaviour at the valve of the pressure and water vapour volume fraction. The flow solver finds the main characteristics of the Water Hammer test case, and compares fairly well with Cathare /ref. 11/ and relap5 numerical results (the Neptune results are denoted “proto_polyphas” in the legend). The saturation pressure, which corresponds to flashing, is well computed and recondensation start at the right time. The pressure peak at the valve at times 0.17 seconds corresponds to the reflexion of a wave coming from the tank after superposition with the wave due to the collapse of the vapour cavity. The mesh comprises 200 cells.

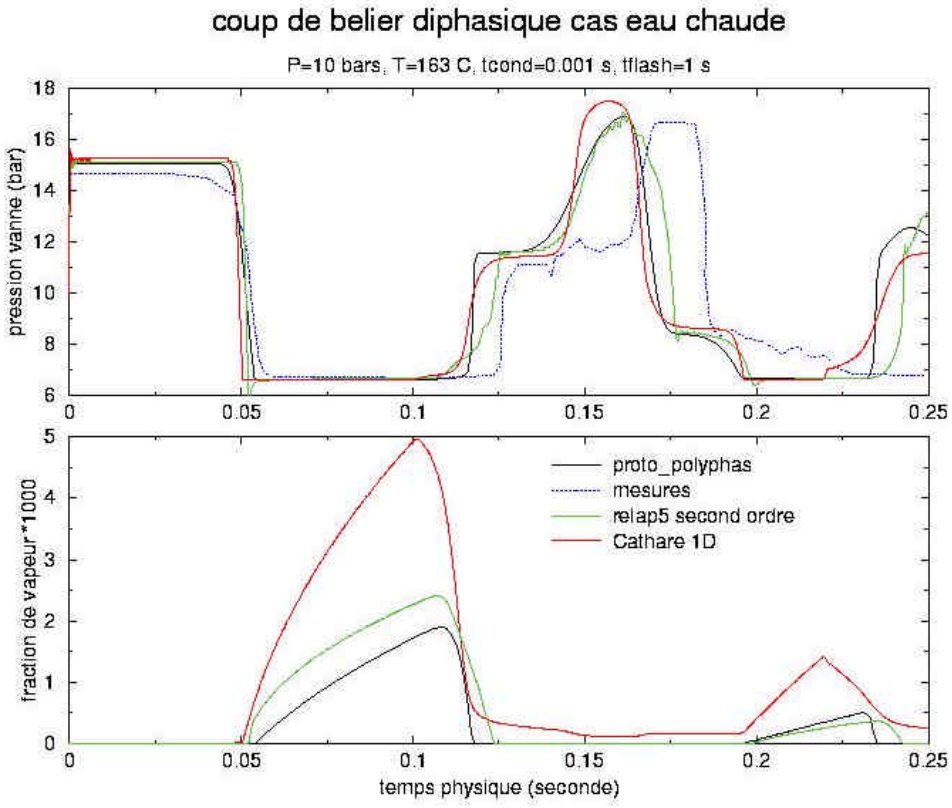

Figure 4
Water Hammer computation

PIERO 2D test case /ref. 12/

This experiment deals with the separation of phases in the lower plenum and the downcomer of a PWR during the end of the depressurization of a large break LOCA. Figure 5 shows the geometry of the experiment. The tank is initially filled of water at rest. The liquid is entrained toward the outlet by an air stream, until an equilibrium level is established, due to the balance between gravity, drag and inertia forces in the downcomer. The final level of water is the experimental result.

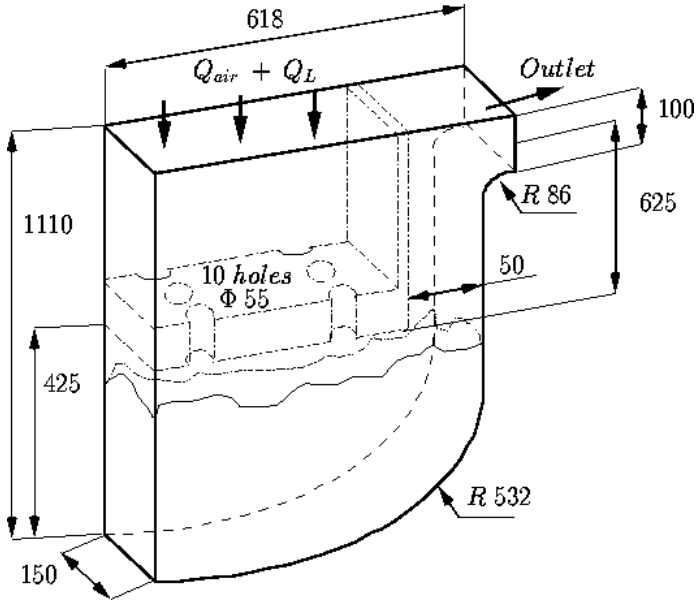

Figure 5
Configuration geometry of the PIERO experiment
(dimensions in millimètre)

The unstructured mesh, comprising 1303 cells of hexahedric and prismatic form, is refined in the downcomer, in order to better predict the interfacial zone between air and water, where water droplets entrainment occurs. The same methodology as in /ref. 13/ has been followed for calculations. From a physical point of view, flow configurations are represented in this manner. From low values of the void fraction (less then 0.3), the flow is considered bubbly. For high values (gerater than 0.7), the flow is considered as dispersed. For intermediate values, two zones, bubbly and dispersed, are defined and smoothly connected with cubic polynomials.

Due to the numerics, the interface is kept in the thickness of about one cell. All computations are performed with second order schemes, with switch to first order schemes, when sharp gradients are detected. This permits to lowerize numerical diffusion and to minimize the number of unphysical values. As no turbulence model is used, the closure laws are subgrid scales models, derived from academic results about droplets and bubbles.

Figure 6 shows the water volume fraction fraction at three times : initial (left), intermediate state with the beginning of droplets entrainment (center) and final state, where an equilbrium level is established (right). It corresponds to the case with air flowrate = 1056 m^3/hour.

Figure 7 shows the unsteady behaviour of the averaged liquid height in the downcomer, for two air flowrates (Q=525, 1056 m^3/hour). This height is deduced from the mass of liquid, staying in the downcomer. Computational results compare fairly well with experimental data and previous calculations performed with the Simmer code /ref. 13/.

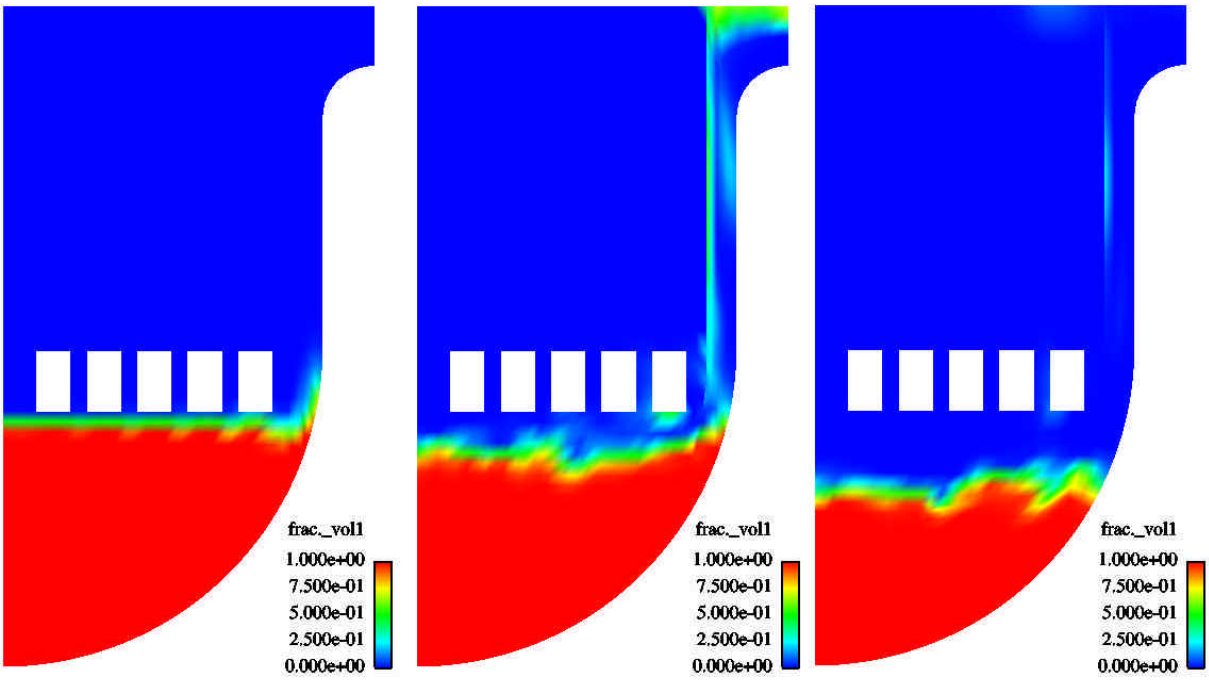

Figure 6
Liquid volume fraction field (in red) at three times
(initial, intermediate and final). Air flowrate = 1056 m3/hour.

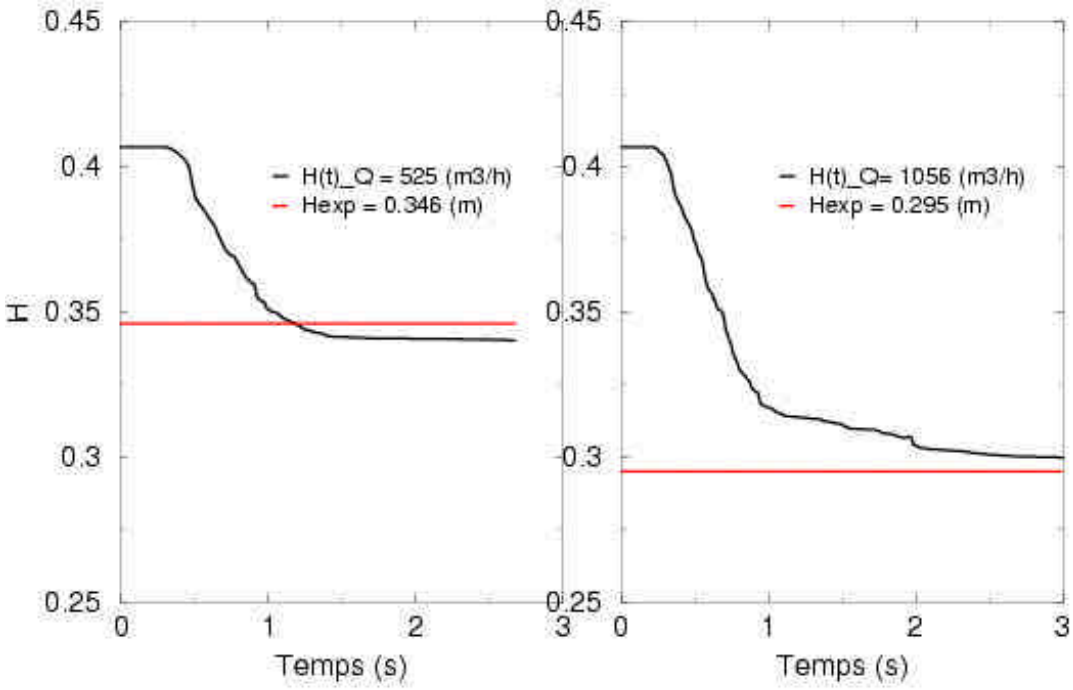

Figure 7
Time evolution of the mean height of the liquid in the downcomer

Conclusion

Based on experience gained at EDF and CEA, a more general and robust 3D multiphase flow solver is being currently developped for over three years. This solver, based on an elliptic oriented fractional step approach, is able to simulate multicomponent/multiphase flows. Each field (fluid component or phase) is modelled through at least 3 conservation equations (mass, momentum and total enthalpy). Additive equations for each field can be used in order to better model physics, as turbulence, phase separation or combustion for instance.

These fields can represent many kind of multiphase flows : distinct physical components (e.g gas, liquid and solid particles) ; thermodynamic phases of the same component (e.g liquid water and its vapour). In order to better predict multifluid physics, a dispersed phase can be split into several components, each component characterized by its own diameter for instance.

The solver is developped in the EDF/CEA NEPTUNE software. Discretization follows a 3D full unstructured finite volume approach, with a collocated arrangement for all variables. A face based data structure allows, in a simple manner, the use of arbitrary shaped cells (tetraedra, hexaedra, prisms, pyramids, ...), including non matching meshes. Numerical consistency and precision for diffusive and advective fluxes for non orthogonal and irregular cells are taken into account through a gradient reconstruction technique. A careful treatment of gradient terms of momentum equations, similar to a Rhie&Chow interpolation, is needed in order to avoid spurious oscillations of pressure, velocity components and volume fractions.

The mass/momentum/energy coupling algorithm can be seen as an extension of the well-known pressure based method used in one phase flow solvers. In our approach, mass and momentum equations are coupled by an iterative procedure within the time step. The non linear behaviour between pressure and volume fractions and a symmetric treatment of all fields are taken into account in the iterative procedure. It greatly enforces the realizability of volume fractions (i.e $0<\alpha<1$), without artificial numerical needs.

Applications to widespread test cases, as static sedimentation, water hammer and phase separation, are shown to assess the robustness of the flow solver in different flow conditions, encountered in nuclear reactor pipes.

Works are still in progress. The presented numerical method has to be improved, in order to take into account more couplings with physical models and to be used for large 3D computations. The directions of some improvements are the followings :

- more lowerize CPU cost by optimizing local and linear systems computations,
- use larger time step by more improving the non linear coupling between mass and momentum,
- use higher order face interpolations, which more minimize at the same time the numerical diffusion and the number of unphysical values.

References

/ref. 1/ C. Béchaud, M. Boucker, A. Douce, M. Grandotto, M. Tadjchman (2003)
A Component Architectur for the Two Phase Flows Simulation Sytem NEPTUNE.
International. Conference On Super Computing in Nuclear Applications, Paris, Sepember 2003.

/ref.2/ N. Méchitoua, M. Boucker, S. Mimouni, S. Pigny, G. Serre (2001)
Numerical simulation of Multiphase flow with an elliptic oriented fractional step method.
Third Int. Symposium on Finite Volume for Complex Applications. Porquerolles, June 2002, France.

/ref. 3/ D. Thaï Van, J.P. Minier, O. Simonin, P. Freydier, J. Olive (1994)
Numerical Method for Multiphase Flows.
ASME Fed, Vol 185, pp 277-291. Lake Taho (USA), 1994.

/ref. 4/ M.B. Carver (1984)
Numerical Computation of Phase Separation in Two Fluid Flow.
Journal of Fluids Engineering, Vol. 106. June 1984.

/ref. 5/ M. Peric (1985)
A Finite Volume Method for the Prediction of Three Dimensional Fluid Flow in Complex Ducts.
PhD Thesis, University of London, August 1985.

/ref. 6/ M. Shashkov, B. Schwartz, B. Wendroff (1998)
Local Reconstruction of a Vector Field from Its Normal Components on the Faces of Grid Cells.
Journal Of Computational Physics 139, pp 406-409 (1998).

/ref. 7/ C.M. Rhie, W.L. Chow (1983)
A Numerical Study of the Turbulent Flow Past an Isolated Airfoil with Trailing Edge Separation.
AIAA Journal, vol. 21, pp 1525-1532 (1983).

/ref. 8/ S. Mimouni, G. Serre (2001)
Physical and Numerical Benchmarks for the computation of Two Phase Liquid-Gas flows.
Internal report EDF/CEA. Note EDF R&D HI-81/01/021/A.

/ref. 9/ H. Paillere, C. Corre, J.R. Cascales Garcia (2001)
On the extension of the AUSM+ Scheme to Compressible Two Fluid Models, *Elsevier Preprint, 2001.*

/ref. 10/ A.R. Simpson (1989)
Large Water Hammer Pressures for column separation in pipelines.
Journal of Hydraulics Engineering, 117, N°10, pp.1310-1316, 1989

/ref. 11/ G. Serre, D. Bestion (2001)
Benchmarks calculated with the ICE numerical method using Cathare and Trio_U codes.
Note CEA/DEN/DTP/SMTH/LMDS/2001-026, Juillet 2001.

/ref. 12/ P. Gully, J.P. Blanc, M. Denux (1983)
Expérience PIERO : étude du phénomène de triage de phases dans le fond de cuve et le downcomer d'un réacteur en fin de décompression accidentelle. *Note CEA-TT/SETRE/69, Août 1983.*

/ref. 13/ S. Pigny, P. Coste (2001)
Two Phase Flow averaged codes : criteria for numerical methods.
International Workshop on Multiphase and Complex Flow Simulation for Industry.
Cargese, September 26-28, France